Regularized Latent Trajectory Models for Spatio-temporal Population Dynamics

Xinyi LU, Yoichiro KANNO, George P. VALENTINE, Matt A. KULP, and Mevin B. HOOTEN

Climate change impacts ecosystems variably in space and time. Landscape features may confer resistance against environmental stressors, whose intensity and frequency also depend on local weather patterns. Characterizing spatio-temporal variation in population responses to these stressors improves our understanding of what constitutes climate change refugia. We developed a Bayesian hierarchical framework that allowed us to differentiate population responses to seasonal weather patterns depending on their "sensitive" or "resilient" states. The framework inferred these sensitivity states based on latent trajectories delineating dynamic state probabilities. The latent trajectories are composed of linear initial conditions, functional regression models, and additive random effects representing ecological mechanisms such as topological buffering and effects of legacy weather conditions. Further, we developed a Bayesian regularization strategy that promoted temporal coherence in the inferred states. We demonstrated our hierarchical framework and regularization strategy using simulated examples and a case study of native brook trout (*Salvelinus fontinalis*) count data from the Great Smoky Mountains National Park, southeastern USA. Our study provided insights into ecological processes influencing brook trout sensitivity. Our framework can also be applied to other species and ecosystems to facilitate management and conservation.

Key Words: Bayesian hierarchical model; State-space model; Functional analysis; Climate change refugia; Brook charr.

X. Lu (✉), Department of Mathematics and Statistics, Utah State University, Logan, UT 84322, USA (E-mail: *lucy.lu@usu.edu*). Colorado Cooperative Fish and Wildlife Research Unit, Colorado State University, Fort Collins, CO 80523, USA.

X. Lu · Y. Kanno · G. P. Valentine, Department of Fish, Wildlife, and Conservation Biology, Colorado State University, Fort Collins, CO 80523, USA.

Y. Kanno · G. P. Valentine, Graduate Degree Program in Ecology, Colorado State University, Fort Collins, CO 80523, USA.

M. A. Kulp, Great Smoky Mountains National Park, U.S. National Park Service, Gatlinburg, TN 37738, USA.

M. B. Hooten, Department of Statistics and Data Sciences, The University of Texas at Austin, Austin, TX 78712, USA.

Journal of Agricultural, Biological, and Environmental Statistics, Volume 30, Number 3, Pages 683–699
https://doi.org/10.1007/s13253-024-00616-y

1. INTRODUCTION

Climate change impacts ecosystems by altering habitat suitability, which in turn threatens species persistence and global biodiversity. The impact varies across space and time due to factors including rates of climate change (Loarie et al. 2009), stability of habitat (Isaac et al. 2008), and ecological/evolutionary adaptation (Bradshaw and Holzapfel 2006; Skelly et al. 2007). Therefore, identifying populations that are less sensitive to the negative impacts of climate change is essential for prioritizing conservation and management efforts (Williams et al. 2008). Population responses to climate change are typically represented by covariate effects in the context of species distribution modeling (Ashcroft 2010; Keppel et al. 2012), and recent studies have revealed evidence of spatial variation in such effects. Kleinhesselink and Adler (2018) showed that sagebrush in colder locations responded positively to above average temperatures while those in hotter locations responded negatively. Scharf et al. (2022) and Raiho et al. (2022) showed that Alaskan plant assemblages responded differently to temperature and precipitation conditioned on geographic features. We developed a state-space model that allowed us to differentiate population responses using "sensitive" and "resilient" states, so that seasonal weather patterns had positive or negative effects on the distribution of "sensitive" populations, and no effect on the distribution of "resilient" populations. Further, we characterized spatio-temporal dynamics in these latent states.

Markov models are commonly used to characterize a sequence of state changes (Zucchini et al. 2017). However, Lu et al. (2023) showed that Discrete Time Markov Chains (DTMCs) are susceptible to imputing unrealistically volatile states, and proposed a class of latent trajectory models that represented dynamic state probabilities instead of state transition probabilities, which were characteristic of DTMCs. A latent trajectory may be considered a spatio-temporal point process in a latent space derived from transformed state probabilities (e.g., via logit or probit link functions). We adopted the latent trajectory framework because shifts between alternative ecosystem states do not constantly occur and are infrequent in many cases (Gunderson 2000; Dakos et al. 2019). Further, we extended the framework by incorporating ecological mechanisms into the components of a latent trajectory. Our specification facilitated inference about factors that may affect population responses: the initial conditions were characterized by landscape features that are variable in space but static in time; temporal dynamics in the direction of "sensitive" were motivated by regional climate change that outpaced species adaptation, and vice versa (Loarie et al. 2009); and auto-correlated random effects were introduced to account for spatial processes such as dispersal potential that influence species persistence (Williams et al. 2008).

Latent trajectory models are flexible in representing spatio-temporal dynamics of state probabilities. However, overparameterization may result from using more parameters than the amount of data. Regularization is a solution to overparameterization that penalizes model complexity to enhance predictive performance. Regularized regression methods are commonly developed for machine learning algorithms that optimize objective functions with tunable penalties (Girosi et al. 1995). On the other hand, Bayesian regularization is attained via prior specification (Burden and Winkler 2009; Hans 2009; Park and Casella 2008; Hooten and Hobbs 2015). Regularizing priors with unique qualities have been established for parameters with continuous support (Williams 1995; Tibshirani 1996; Polson and Scott

2010), but there are few studies concerning regularization of parameters with discrete support. We developed a novel Bayesian regularization strategy to promote temporal coherence in the inferred binary states. Although smoothness in state probabilities may be induced by temporally correlated covariates or basis functions (Hefley et al. 2017), the states generated from these probabilities may still be variable. For example, there is likely higher temporal variation in a sequence of states generated from independent Bernoulli distributions conditioned on a constant sequence of probability 0.5. Therefore, we specified a joint distribution for the sequence of latent states that penalizes the number of state transitions.

Past climate conditions can influence current species distributions. For example, long-lived species such as trees demonstrate years of "ecological memory" in response to legacy conditions (Ogle et al. 2015; Johnstone et al. 2016). Even for short-lived species such as stream fish, population recovery from fires and floods can take generations (Dunham et al. 2003). Characterizing a scalar response using a sequence of covariates observed over time is a form of functional data analysis (FDA), specifically, functional predictor regression (scalar-on-function) (Morris 2015). Functional predictor regression has the common form of $\tilde{y}_i = \tilde{\beta}_0 + \int \tilde{x}_i(t)\tilde{\beta}(t)\mathrm{d}t + \tilde{\epsilon}_i$, where the coefficients, $\tilde{\beta}(t)$, and/or the predictors, $\tilde{x}_i(t)$, are modeled using basis function expansions (Ramsay and Dalzell 1991; Hastie and Mallows 1993). A special case of functional predictor regression are distributed lag models (DLMs), where an outcome is represented by the summation of the current and lagged covariate with temporally varying coefficients (Warren et al. 2012b; Mork and Wilson 2022). Previous examples of DLMs in ecology relied on specific lags whose coefficients were estimated independently (Ogle et al. 2015; Peltier et al. 2018). We specified a mechanistic function that correlated the lagged coefficients, thereby facilitating interpretability and numerical stability.

We presented our method in Sect. 2. In Sect. 3, we demonstrated the method using a case study of native brook trout (*Salvenilus fontinalis*) count data from the Great Smoky Mountains National Park, southeastern USA. Finally in Sect. 4, we discussed possible extensions and broader applications of our method.

2. METHOD

2.1. HIERARCHICAL FRAMEWORK

Our hierarchical framework consisted of data, process, and parameter models following the convention of Berliner (1996) and Wikle et al. (1998). We denoted $y_{i,t,j}$ the observed count at site i, $i = 1, \ldots, n$, in year t, $t = 1, \ldots, T$, during electrofishing pass j, $j = 1, \ldots, J$. Our data were collected under a depletion sampling protocol, where each site was sampled repeatedly (for J passes), and captured individuals at each pass were separated from the population during subsequent passes. The data model represented the protocol as follows,

$$y_{i,t,j} \sim \begin{cases} \text{Binomial}\left(N_{i,t},\ p\right), & j = 1, \\ \text{Binomial}\left(N_{i,t} - \sum_{l=1}^{j-1} y_{i,t,l},\ p\right), & j > 1, \end{cases} \tag{1}$$

where $N_{i,t}$ was the true abundance at site i, in year t, and p was the capture probability. Further, we specified

$$N_{i,t} \sim \text{Poisson}(A_i \lambda_{i,t}), \tag{2}$$

where A_i was the survey area of site i, and $\lambda_{i,t}$ was the population density at site i, in year t. The data model was an adaptation of the N-mixture framework (Royle 2004) that accounted for imperfect detection and inferred true abundance by assuming population closure and homogeneous capture probability among individuals.

In the process model, we characterized population density using a log-linear function of covariates as follows,

$$\log\left(\lambda_{i,t}\right) = \boldsymbol{x}_i'\boldsymbol{\beta} + \boldsymbol{h}_{i,t}'\tilde{\boldsymbol{\theta}}_{i,t}. \tag{3}$$

The predictor variable $\boldsymbol{x}_i = \left(x_{i,1}, \ldots, x_{i,Q_X}\right)'$ represented landscape covariates at site i, where Q_X was the total number of landscape covariates; and $\boldsymbol{h}_{i,t} = \left(h_{i,t,1}, \ldots, h_{i,t,Q_H}\right)'$ represented weather covariates at site i, in year t, where Q_H was the total number of weather covariates. To account for different population responses, we let $\tilde{\boldsymbol{\theta}}_{i,t} = \left(\tilde{\theta}_{i,t,1}, \ldots, \tilde{\theta}_{i,t,Q_H}\right)'$ vary by site and year for each weather covariate. We denoted $z_{i,t,q}$ the latent state at site i, in year t, for the qth weather covariate, $q = 1, \ldots, Q_H$, where $z_{i,t,q} = 1$ represented "sensitive" and $z_{i,t,q} = 0$ represented "resilient." We specified that $\tilde{\theta}_{i,t,q} = \theta_q \times z_{i,t,q}$, so that $\tilde{\theta}_{i,t,q} = \theta_q \sim \text{N}\left(0, \sigma_q^2\right)$ when the population was sensitive at site i, in year t, toward the qth weather covariate; and $\tilde{\theta}_{i,t,q} = 0$ if the population was resilient at site i, in year t, against the qth weather covariate. In other words, the probability of the qth weather covariate having a non-zero effect on density was one when $z_{i,t,q} = 1$, and the probability was zero when $z_{i,t,q} = 0$. We modeled the sequence of states at site i for the qth weather covariate, $\boldsymbol{z}_{i,q} = \left(z_{i,1,q}, \ldots, z_{i,T,q}\right)'$, as Bernoulli random variables whose joint distribution depended on state probabilities and a regularization term that penalizes state switching. We introduced the joint distribution of $\boldsymbol{z}_{i,q}$ in Sect. 2.2, and completed the process model by specifying the latent state probability at site i, in year t, for the qth weather covariate, $\rho_{i,t,q}$, using a latent trajectory representation as follows,

$$\text{logit}\left(\rho_{i,t,q}\right) = \underbrace{\boldsymbol{m}_i'\boldsymbol{v}_q}_{\text{Initial Conditions}} + \underbrace{\sum_{\tau=1}^{t} w_{i,q}(\tau)\delta(\boldsymbol{\xi}_q, \tau)}_{\text{Driver Effect}} + \underbrace{\epsilon_{i,t,q}}_{\text{Random Effect}}. \tag{4}$$

The variable $\boldsymbol{m}_i = \left(m_{i,1}, \ldots, m_{i,Q_M}\right)'$ represented landscape features that are temporally static over the study period, where Q_M was the total number of landscape features (for latent trajectory); and $\boldsymbol{v}_q = \left(v_{q,1}, \ldots, v_{q,Q_M}\right)'$ represented interactive effects between these features and the qth weather covariate. The product $\boldsymbol{m}_i'\boldsymbol{v}_q$ defined the initial condition of the latent trajectory at site i for the qth weather covariate, and represented a baseline against which subsequent progression in time was measured. The summation indicated the cumulative effect from present and past driver conditions at site i, up to year t, for

the qth weather covariate, where $\boldsymbol{w}_{i,q} = (w_{i,q}(1), \ldots, w_{i,q}(t))'$, $\delta(\cdot)$ denoted the driver coefficients, and τ was a temporal index on the summands. We specified for the qth weather covariate that its driver effect in year t was,

$$\delta(\boldsymbol{\xi}_q, \tau) = \alpha_q \exp(-(t-\tau)/\psi_q), \tag{5}$$

where $\boldsymbol{\xi}_q \equiv (\alpha_q, \psi_q)'$. According to Eq. 5, α_q represented the present driver effect when $\tau = t$, and had the largest magnitude among all coefficients; the lagged driver effects decayed exponentially in magnitude while maintaining the same direction as α_q, where ψ_q indicated the rate of decay.

Lastly, we specified spatially correlated random effects in year t for the qth weather covariate,

$$\boldsymbol{\epsilon}_{t,q} \sim \mathrm{N}(\mathbf{0}, \sigma_q^2 \exp(-\boldsymbol{D}/\phi_q)), \tag{6}$$

where $\boldsymbol{D}$ represented geodesic distances between pairs of sites, and "exp" was an element-by-element exponential. We completed the hierarchy by specifying prior distributions in our parameter model. For the case study, we assigned informative priors to capture probabilities based on a previous study (Kanno et al. 2015) and diffuse priors to the other parameters. For the population level parameters, we let $p_{\mathrm{YOY}} \sim \mathrm{Beta}(6, 4)$, $p_{\mathrm{Adult}} \sim \mathrm{Beta}(7, 3)$, $\boldsymbol{\beta} \sim \mathrm{N}\left(\mathbf{0}, \mathbf{I}_{Q_X \times Q_X}\right)$, and $\theta_q \sim \mathrm{N}(0, 1)$ for $q = 1, \ldots, Q_H$. For the latent trajectory parameters, we let $\boldsymbol{v}_q \sim \mathrm{N}\left(\mathbf{0}, \mathbf{I}_{Q_M \times Q_M}\right)$, $\alpha_q \sim \mathrm{N}(0, 1)$, $\psi_q \sim \mathrm{Unif}(0, 10)$, $\phi_q \sim \mathrm{Unif}(0, 20)$, and $\log \sigma_q \sim \mathrm{N}(0, 1)$, for $q = 1, \ldots, Q_H$.

2.2. BAYESIAN REGULARIZATION

In our study, estimating latent states was challenged by the non-Gaussian data, the hierarchies of the modeling framework, and the state themselves being binary. Therefore, we developed a regularization strategy to improve estimation by assuming temporal coherence and penalizing changes in the sequence of states. We defined

$$\left[\boldsymbol{z}_{i,q} | \boldsymbol{\rho}_{i,q}, a, c\right]_{\mathrm{reg}} \propto \frac{\prod_{t=1}^{T} \left[z_{i,t,q} | \rho_{i,t,q}\right]}{\left(||\boldsymbol{z}_{i,2:T,q} - \boldsymbol{z}_{i,1:T-1,q}||_1 + a\right)^c}, \tag{7}$$

where $\boldsymbol{\rho}_{i,q} = \left(\rho_{i,1,q}, \ldots, \rho_{i,T,q}\right)'$, $\boldsymbol{z}_{i,2:T,q} = \left(z_{i,2,q}, \ldots, z_{i,T,q}\right)'$, and $\left[z_{i,t,q} | \rho_{i,t,q}\right] = \mathrm{Bern}\left(\rho_{i,t,q}\right)$. The $\mathcal{L}_1$ norm accounted for the number of change points in $\boldsymbol{z}_{i,q}$. The additive parameter $a > 0$ ensured a valid likelihood in the case of no change point, and the tuning parameter $c \geq 0$ down-weighted the joint likelihood as the number of change points increases. When $T < \infty$, the exact probability of $\boldsymbol{z}_{i,q}$ given $\boldsymbol{\rho}_{i,q}$, a, and c can be derived as follows,

$$\mathbb{P}\left(\boldsymbol{z}_{i,q} | \boldsymbol{\rho}_{i,q}, a, c\right) = \frac{\left[\boldsymbol{z}_{i,q} | \boldsymbol{\rho}_{i,q}, a, c\right]_{\mathrm{reg}}}{\sum_{\tilde{z} \in \mathcal{Z}} [\tilde{z} | \boldsymbol{\rho}_{i,q}, a, c]_{\mathrm{reg}}},$$

where $\mathcal{Z}$ represented the set of all possible permutations of $\boldsymbol{z}_{i,q}$. Because the summation was $\mathcal{O}\left(2^T\right)$ and computationally prohibitive with large T, we derived the full-conditional distribution of $z_{i,t,q}$ to facilitate sequential update in a Markov chain Monte Carlo (MCMC) algorithm,

$$\left[z_{i,t,q}|\rho_{i,t,q}, \boldsymbol{z}_{i,-t,q}, a, c\right]_{\text{reg}} = \text{Bern}\left(\tilde{\rho}_{i,t,q}\right), \tag{8}$$

where $\boldsymbol{z}_{i,-t,q} = \left(z_{i,1,q}, \ldots, z_{i,t-1,q}, z_{i,t+1,q}, \ldots, z_{i,T,q}\right)'$ and

$$\tilde{\rho}_{i,t,q} = \frac{\rho_{i,t,q} / \left(|1 - z_{i,t-1,q}| + |z_{i,t+1,q} - 1| + a + b\right)^c}{\rho_{i,t,q} / \left(|1 - z_{i,t-1,q}| + |z_{i,t+1,q} - 1| + a + b\right)^c + \left(1 - \rho_{i,t,q}\right) / \left(z_{i,t-1,q} + z_{i,t+1,q} + a + b\right)^c},$$
$$b = ||\boldsymbol{z}_{i,2:t-1,q} - \boldsymbol{z}_{1,1:t-2,q}||_1 + ||\boldsymbol{z}_{i,t+2:T,q} - \boldsymbol{z}_{i,t+1:T-1,q}||_1.$$

The full-conditional distribution of $z_{i,t,q}$ in a hierarchical model was still Bernoulli, where the numerator and the denominator incorporated the appropriate data-specific distributions.

To demonstrate, we specified a binary sequence, $\boldsymbol{z} = (z_1, \ldots, z_T)'$, $T = 100$, where the first fifty elements were zero and the last fifty elements were one. The sequence may be considered a random vector generated from a Dirac delta distribution whose probability mass was one at the said specification and zero everywhere else. We simulated count data conditioned on $\boldsymbol{z}$ as follows,

$$N_t \sim \text{Pois}(\mu_t),$$
$$\log(\mu_t) = \left(\boldsymbol{x}_t'\boldsymbol{\beta}\right) z_t,$$

for $t = 1, \ldots, T$, where elements of $\boldsymbol{x}_t = \left(x_{1,t}, x_{2,t}\right)'$ were independent standard normal variables, and $\boldsymbol{\beta} = (1, 0.5)'$. Typical simulation studies achieve model validation by showing that the model can recover true parameters based on the same set of assumptions that generated data. However, in reality, highly complex ecological processes may prevent us from specifying the exact mechanisms governing state changes. Therefore, we demonstrated that our regularized joint likelihood (Eq. 7) assisted in recovering $\boldsymbol{z}$ under reasonable assumptions that $[z_t|\rho_t] = \text{Bern}(\rho_t)$ and $\text{logit}(\rho_t) = \alpha_0 + \alpha_1 t$, without knowledge of the generating distribution of $\boldsymbol{z}$.

The tuning process of our regularization strategy required evaluating model predictive performance on various values of c via cross-validation. According to Eq. 7, optimal tuning may depend on the length of $\boldsymbol{z}$ because longer sequences may host more change-points. In practice, we recommend selecting initial candidate c values that encompass a range of numerical orders, and repeating the validation process iteratively for narrower ranges of $\boldsymbol{c}$ until different penalties do not produce qualitatively different inference on $\boldsymbol{z}$. Figure 1 illustrated posterior samples of $\boldsymbol{z}$ under various penalties from the array $\boldsymbol{c} = (0, 1, 10, 100)'$. We conducted a three-fold cross-validation for every element of $\boldsymbol{c}$. At each non-overlapping fold, we randomly designated two-thirds of the simulated counts as the training set and the remaining one-third as the test set. We fit the model to the training set to obtain posterior samples of $\boldsymbol{\beta}$ and predictive samples of $\boldsymbol{z}$, with which we evaluated posterior predictive

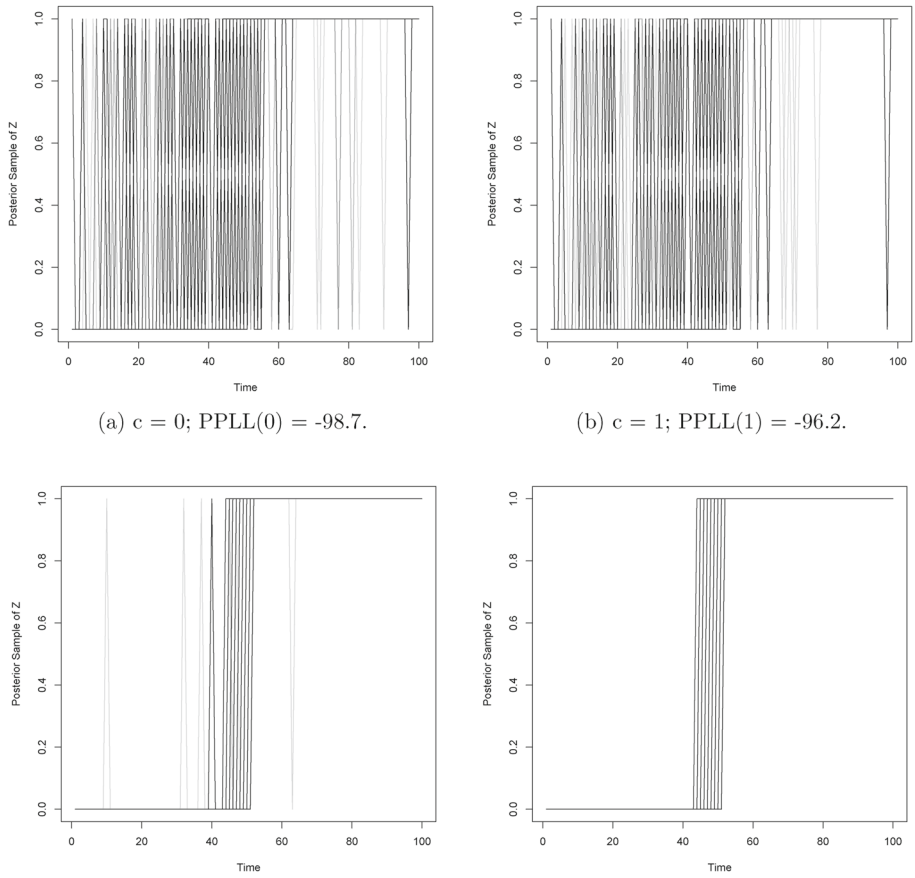

(a) c = 0; PPLL(0) = -98.7.

(b) c = 1; PPLL(1) = -96.2.

(c) c = 10; PPLL(10) = -63.4.

(d) c = 100; PPLL(100) = -63.3.

Figure 1. Posterior samples of inferred z under different penalties and the associated predictive scores for the simulated example. A higher score indicates better performance.

log likelihood (PPLL) on the test set. The predictive scores were averaged over folds and MCMC iterations as follows,

$$\begin{aligned}\text{PPLL}(c) &= \frac{1}{R}\sum_{r=1}^{R}\log\left[\boldsymbol{N}_{\text{Test},r}|\boldsymbol{N}_{\text{Train}},\ c\right] \\ &= \frac{1}{R}\sum_{r=1}^{R}\frac{1}{K}\sum_{k=1}^{K}\log\left\{\left[\boldsymbol{N}_{\text{Test},r}|\boldsymbol{\beta}^{(k)},\boldsymbol{z}^{(k)}_{\text{Pred},r}\right]\left[\boldsymbol{\beta}^{(k)},\boldsymbol{z}^{(k)}_{\text{Pred},r}|\boldsymbol{N}_{\text{Train},r},\ c\right]\right\},\end{aligned}$$

where R denotes the number of folds, and K denotes the number of MCMC iterations. Because the inferred z sequences were most precise around the truth for $c = 100$, and PPLL(100) was the highest among all penalties, we selected the optimal penalty to be $c^* = 100$ for the above example.

3. APPLICATION

3.1. DATA

Brook trout populations have experienced substantial declines throughout their native range in eastern North America (Hudy et al. 2008). A short-lived cold-water species, brook trout spawn during fall and hatch in late winter to early spring (Hazzard 1932). Brook trout are sensitive to alterations in stream temperature and flow among various environmental stressors. High summer temperatures can cause physiological stress and negatively affect spawning (Xu et al. 2010b; Warren et al. 2012a), and high flows can cause bed scouring events that increase mortality of eggs and larval fish (Roghair et al. 2002; Kanno et al. 2015).

We analyzed brook trout count data from 33 sites in the Great Smoky Mountains National Park (GRSM), southeastern USA, between 1980 and 2015. Data were collected using electrofishing surveys that occurred between June and October. The sites were not surveyed annually, and we selected sites with five or more years of data that allowed us to study temporal dynamics. Surveys were conducted using a depletion sampling protocol, where block nets or natural barriers were used to ensure population closure during sampling, and three successive upstream-electrofishing passes were conducted with one backpack electrofisher and one netter every three meters of stream width. Captured brook trout were weighed (g) and measured (mm), and identified as young-of-the-year (YOY, $\leq$ 90 mm) and adult ($>$ 90 mm) (Habera et al. 2010; Kanno et al. 2017).

For the landscape covariates, $\boldsymbol{x}_i$ (Eq. 3), we used an intercept, latitude, and elevation; and the same covariates were used for $\boldsymbol{m}_i$ (Eq. 4). Latitude and elevation are known drivers of brook trout abundance (Kanno et al. 2015) and were standardized over the study region. For the weather covariates, $\boldsymbol{h}_{i,t}$ (Eq. 3), we used high summer temperature of previous year and high winter flows of present year. We obtained estimates of daily maximum temperatures at a 1 km$\times$1 km spatial resolution from DAYMET (Thornton et al. 2022), and averaged the daily estimates between June and September to derive high summer temperatures at each site. We obtained monthly flow estimates from National Hydrography Dataset Plus (NHDPlus) (U.S. Geological Survey 2016), and used the 90th flow percentiles between December and February to represent high winter flows at each site. The weather covariates were standardized by site over the study period to reflect relative temporal variation in local weather patterns. For the latent trajectory drivers associated with weather, $w_{i,q}(\tau)$ (Eq. 4), we hypothesized that summer precipitation drives population responses to summer temperature, and extreme winter flow drives population responses to high winter flow. Extreme flows represented potential flood events capable of altering habitat structures (e.g., channel morphology) in the long term. These events accounted for around 2% of the sampling sites and years, and they were not highly correlated with the corresponding seasonal flows (pairwise Pearson's correlations $<$ 0.35). We obtained and standardized summer precipitation from DAYMET similarly to temperature, and we defined extreme winter flows as indicator variables for flows greater than 2.5 site-specific standard deviations.

Table 1. Summary of marginal posterior means (95% credible intervals) under the optimal tuning parameter, for YOY and adult, respectively

Parameter	YOY	Adult
p (Capture Prob.)	0.58 (0.57, 0.59)	0.70 (0.69, 0.70)
β_0 (Intercept)	3.72 (3.70, 3.75)	3.88 (3.86, 3.90)
β_1 (Latitude)	− 0.12 (− 0.15, − 0.10)	0.01 (− 0.02, 0.05)
β_2 (Elevation)	0.46 (0.43, 0.48)	0.72 (0.69, 0.75)
θ_1 (Summer Temperature)	− 1.38 (− 1.42, − 1.34)	− 1.33 (− 1.37, − 1.28)
θ_2 (Winter Flow)	− 0.97 (− 1.00, − 0.94)	− 0.87 (− 0.90, − 0.84)
$\nu_{1,1}$ (Intc. × Sum. Temp.)	− 0.41 (− 0.63, − 0.19)	− 0.81 (− 1.06, − 0.60)
$\nu_{1,2}$ (Lat. × Sum. Temp.)	− 0.04 (− 0.35, 0.27)	0.29 (− 0.04, 0.60)
$\nu_{1,3}$ (Elev. × Sum. Temp.)	− 0.24 (− 0.49, 0.04)	0.13 (− 0.16, 0.43)
$\nu_{2,1}$ (Intc. × Win. Flow)	− 0.63 (− 0.85, − 0.42)	− 0.55 (− 0.76, − 0.33)
$\nu_{2,2}$ (Lat. × Win. Flow)	0.18 (− 0.13, 0.49)	0.22 (− 0.07, 0.57)
$\nu_{2,3}$ (Elev. × Win. Flow)	0.09 (− 0.20, 0.37)	− 0.09 (− 0.37, 0.22)
α_1 (Drv. Conc. Sum. Temp.)	− 0.14 (− 0.40, 0.08)	− 0.37 (− 0.58, − 0.10)
α_2 (Drv. Conc. Win. Flow)	− 0.05 (− 0.35, 0.27)	− 0.32 (− 0.75, 0.13)
ψ_1 (Drv. Range Sum. Temp.)	2.46 (0.02, 9.02)	0.73 (0.03, 4.16)
ψ_2 (Drv. Range Win. Flow)	7.88 (2.73, 9.89)	4.85 (0.62, 8.98)
σ_1^2 (Spat. Var. Sum. Temp.)	0.02 (0.02, 0.03)	0.01 (0.01, 0.02)
σ_2^2 (Spat. Var. Win. Flow)	0.02 (0.02, 0.03)	0.04 (0.03, 0.04)
ϕ_1 (Spat. Range Sum. Temp.)	2.68 (2.20, 3.32)	2.75 (2.27, 3.29)
ϕ_2 (Spat. Range Win. Flow)	4.12 (3.30, 5.26)	5.73 (4.56, 6.76)

3.2. CASE STUDY

We implemented our model using an MCMC sampling algorithm in R, and demonstrated in simulation (Appendix A) the capacity of our full hierarchical model (Sect. 2.1). We fit the model separately for YOY and adult, and ran the algorithm for 20,000 iterations with the first 10,000 burn-in samples discarded. We set $a = 1$ and selected the tuning parameter, c, using the procedure described in Sect. 2.2. Composition sampling is commonly used to evaluate predictive scores for hierarchical models, as is exemplified below,

$$\left[\boldsymbol{y}_{\text{Test}}|\boldsymbol{y}_{\text{Train}}, c\right] = \int_p \int_{\boldsymbol{\lambda}_{\text{Pred}}} \sum_{\boldsymbol{N}_{\text{Pred}}} \left[\boldsymbol{y}_{\text{Test}}|\boldsymbol{N}_{\text{Pred}}, p\right] \left[\boldsymbol{N}_{\text{Pred}}|\boldsymbol{\lambda}_{\text{Pred}}\right] \left[\boldsymbol{\lambda}_{\text{Pred}}, p|\boldsymbol{y}_{\text{Train}}, c\right] d\boldsymbol{\lambda}_{\text{Pred}} \mathrm{d}p,$$

However, a particular challenge to this calculation in our case study arose because predictive samples of true abundance may be smaller than the observed counts in the test set (i.e., $\boldsymbol{N}_{\text{Pred}} < \boldsymbol{y}_{\text{Test}}$). To circumvent sampling $\boldsymbol{N}_{\text{Pred}}$, we used the integrated likelihood,

$$\left[\boldsymbol{y}_{\text{Test}}|\boldsymbol{\lambda}_{\text{Pred}}, \ p\right] = \sum_{\boldsymbol{N}=\boldsymbol{y}_{\text{Test}}}^{\infty} \left[\boldsymbol{y}_{\text{Test}}|\boldsymbol{N}, p\right] \left[\boldsymbol{N}|\boldsymbol{\lambda}_{\text{Pred}}\right],$$

and a large upper bound for $\boldsymbol{N}$ to approximate summation to infinity. The optimal tuning parameters were selected to be $c^* = 1.5$ for YOY, and $c^* = 2$ for adult. Table 1 summarized the estimated marginal posterior distributions from the best predictive models.

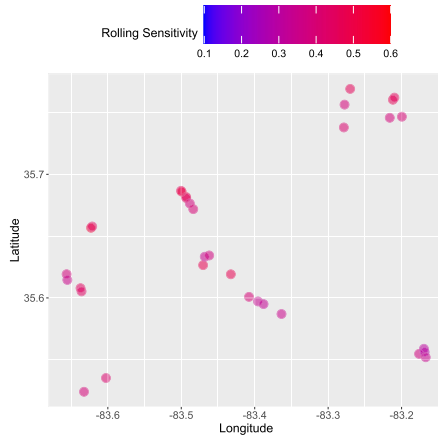

(a) YOY sensitivity to high summer temperature.

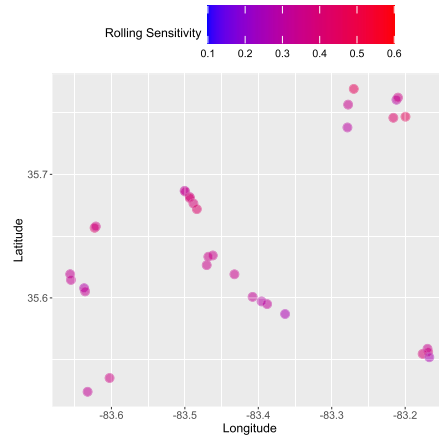

(b) YOY sensitivity to high winter flow.

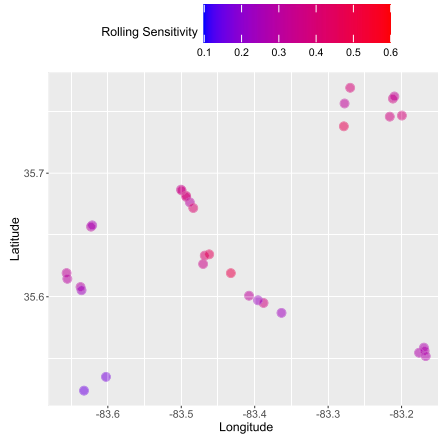

(c) Adult sensitivity to high summer temperature.

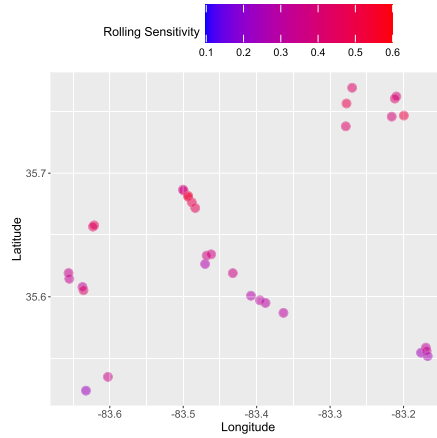

(d) Adult sensitivity to high winter flow.

Figure 2. Maps of posterior mean rolling sensitivities by life stage and weather covariate.

Our estimated capture probabilities demonstrated high precision and conformed with estimates from a previous study (Kanno et al. 2015) (Table 1). Latitude negatively affected YOY abundance (−0.12 (−0.15, −0.10)), and elevation positively affected both YOY (0.46 (0.43, 0.48)) and adult (0.72 (0.69, 0.75)) abundance. For populations inferred as "sensitive," both weather covariates affected abundance adversely, with summer temperature (YOY: −1.38 (−1.42, −1.34); Adult: −1.33 (−1.37, −1.28)) resulting in more severe impact than winter flow (YOY: −0.97 (−1.00, −0.94); Adult: −0.87 (−0.90, −0.84)). Within the latent trajectory model, the landscape features used to investigate interaction with local weather patterns did not reveal any significant effect. Among the drivers, summer precipitation decreased adult sensitive probability to high temperature (−0.37 (−0.58, −0.10)). Extreme winter flows did not significantly affect YOY or adult sensitive probability to high flows. The posterior mean temporal ranges of the drivers were shorter for summer temperature (YOY: 2.46 (0.02, 9.02); Adult: 0.73 (0.03, 4.16)) than for winter flow (YOY: 7.88 (2.73, 9.89);

Adult: 4.85 (0.62, 8.98)), although the posterior variances were high. The spatial variances of the random effects were comparable across life stages and weather covariates. The posterior mean spatial ranges of the random effects were shorter for summer temperature (YOY: 2.68 (2.20, 3.32); Adult: 2.75 (2.27, 3.29)) than for winter flow (YOY: 4.12 (3.30, 5.26); Adult: 5.73 (4.56, 6.76)), and the posterior variances were low. We denoted "rolling sensitivity" the average of the inferred latent states over time at each site (Fig. 2). The maps demonstrated similar patterns across life stages and covariates, where the clusters of sites in the southeast and southwest of the study region showed lower rolling sensitivities.

4. DISCUSSION

We developed a statistical framework that quantified spatio-temporal heterogeneity in population responses to seasonal weather patterns. We used a latent trajectory specification to study the effects of topological buffering and legacy weather conditions on changes between "sensitive" and "resilient" states. We demonstrated our framework using a case study of native brook trout count data. Our model indicated that precipitation mitigated adult sensitivity to summer heat, possibly because rainfall lowered stream temperature and increased habitat volume and access to thermally suitable locations such as small tributaries (Xu et al. 2010a; Merriam et al. 2017). The relief, however, was not evident among YOY, possibly because juvenile fish were able to utilize small habitat space and shallow pools during dry summers (Hakala and Hartman 2004). Many agencies are implementing brook trout restoration projects across their native range (Kanno et al. 2016; Wood et al. 2018). Although any newly restored habitat is important to overall species survival, managers should consider population responses to summer temperature prior to restoration, and carefully decide whether to restore stream segments approaching upper temperature tolerance where populations also demonstrate high sensitivity. Extreme winter flows were not found to be a significant driver of flow sensitivity, potentially due to the scarcity of such events. Nonetheless, the estimated temporal range suggested that precedent flood events could have longer-lasting impact than precedent summer conditions (Elwood and Waters 1969; Carline and McCullough 2003). The estimated ranges of spatial correlation also suggested that when conditioned on the covariates, temperature sensitivity demonstrated more localized patterns than flow sensitivity, likely due to surface-ground-water interactions (Hare et al. 2023).

Our regularization strategy promoted temporal coherence in the inferred latent states. The penalty term defined as a tunable weight on the original joint likelihood (Eq. 7; i.e., $\log[\boldsymbol{z}_{i,q}|\boldsymbol{\rho}_{i,q}, a, c] = [\boldsymbol{z}_{i,q}|\boldsymbol{\rho}] - cf(\boldsymbol{z}_{i,q}, a, c)$) provided a Bayesian representation of a customary loss function involving non-Gaussian variables (Jia et al. 2021; Wadsworth et al. 2018). Besides tuning c, the strength of penalty also depends on the norm and the additive parameter, a. However, simultaneously tuning all three elements may result in confounding. Future studies can investigate behaviors of the regularized likelihood by tuning each element separately. As is illustrated by the example in Sect. 2.2, the regularized likelihood is non-generative and based on reasonable assumptions about state changes; therefore, a zero penalty does not imply true independence in $\boldsymbol{z}$, and a non-zero penalty does not imply true dependence. In our simulation study (Appendix A), the latent states were generated from

Table 2. Summary of true parameters with associated marginal posterior distributions from one simulation and empirical coverage from twenty simulations

Parameter	True	Posterior Mean (95% CI)	Empirical Coverage
p	0.7	0.70 (0.68, 0.71)	0.95
β_0	2	2.05 (1.99, 2.13)	0.85
β_1	− 1	− 0.96 (− 1.00, − 0.91)	0.9
β_2	0.5	0.51 (0.46, 0.56)	0.95
θ_1	− 0.8	− 0.82 (− 0.85, − 0.79)	0.95
θ_2	− 1.2	− 1.18 (− 1.24, − 1.12)	0.8
$\nu_{1,1}$	1	2.19 (1.11, 3.32)	0.75
$\nu_{1,2}$	− 1	− 0.74 (− 2.04, 0.43)	0.65
$\nu_{1,3}$	2	3.21 (2.32, 4.11)	0.9
$\nu_{2,1}$	− 1	− 0.28 (− 1.24, 0.62)	0.9
$\nu_{2,2}$	1	2.44 (1.51, 3.52)	0.6
$\nu_{2,3}$	− 0.5	− 0.64 (− 1.36, − 0.04)	0.95
α_1	− 0.5	− 0.08 (− 0.52, 0.28)	0.5
α_2	− 0.3	− 0.08 (− 0.65, 0.31)	0.6
ψ_1	3	2.83 (0.14, 4.92)	1
ψ_2	3	2.03 (0.12, 4.70)	1
σ_1^2	0.01	0.01 (0.01, 0.03)	0.8
σ_2^2	0.01	0.01 (0.01, 0.02)	0.6
ϕ_1	3	3.65 (2.08, 4.87)	0.8
ϕ_2	3	3.93 (2.47, 4.97)	0.85

independent Bernoulli distributions; however, the optimal tuning parameters may be selected to be non-zero. Posterior inference from one simulation and empirical coverage from multiple simulations (Table 2) indicated that our model was able to recover parameters on abundance ($p, \boldsymbol{\beta}, \boldsymbol{\theta}$) with close to nominal coverage. In comparison, several parameters on initial conditions, concurrent driver effects, and spatial random effects ($\nu_{1,1}, \nu_{1,2}, \nu_{2,2}, \alpha_1, \alpha_2, \sigma_2^2$) had lower empirical coverage. Inferring latent trajectory parameters is challenging, even in the absence of regularization, because the states are discrete (Lu et al. 2023). Longer and more complete time series may reduce bias and increase precision in these parameters; nonetheless, we kept the simulation scale similar to that of our case study to realistically demonstrate the capabilities and limitations of our framework. The ecological conclusions we drew were supported both by posterior inference from the model and previous studies on relevant systems.

A possible extension to our regularization in time is to regularize in space or space-time. The conditional likelihood of $z_{i,t,q}$ is based on the element's similarity within its local neighborhood relative to the sequence's overall homogeneity (Eq. 8). This concept also guides behaviors of statistical mechanic models such as Ising and Potts models in two-dimensional space (Glauber 1963; Wu 1982). A regularizing distribution that penalizes roughness in space could take the following form

$$\left[\boldsymbol{z}_{t,q}|\boldsymbol{\rho}_{t,q}, a, c\right]_{\text{reg}} \propto \frac{\prod_{i=1}^{n}\left[z_{i,t,q}|\rho_{i,t,q}\right]}{\left(\sum_{i=1}^{n}\sum_{j\in\mathcal{N}_i}||z_{i,t,q}-z_{i,j,q}||+a\right)^{c}},$$

where $\mathcal{N}_i$ denotes the neighborhood of i with typical choices of Queen, Rook, or Delaunay triangulation neighborhoods (Felus et al. 2005; Griffith 2020). A regularizing distribution in space-time could penalize a weighted combination of change points in both spatial and temporal dimensions. Further, our regularizing strategy can extend to multiple states. The joint distribution of $\boldsymbol{z}_{i,q}$ could retain Eq. 7, where $z_{i,t,q}$ will be ordinal variables (e.g., 1 = less sensitive, 2 = sensitive, 3 = more sensitive), and the conditional distribution of $z_{i,t,q}$ will be multinomial.

A future direction of our case study is to incorporate more detailed landscape features and to expand the analysis by synthesizing data across the southeast United States. Enriched data may require more flexible models to account for additional sources of variation. For example, we can model heterogeneity in capture probabilities using covariates on data source, sampling protocol, and segment condition prior to sampling (Johnson et al. 2010; Fletcher et al. 2019; Farr et al. 2021; Mohankumar et al. 2023). We can allow over-dispersion and induce autocorrelation in the data model using spatial and/or temporal random effects to characterize log density (Chakraborty et al. 2011; Renner et al. 2015). We can also specify the latent trajectory model to represent complex population dynamics such as density-regulated growth and competition. Our latent trajectory specification is applicable to most state-space models in econometrics (Hamilton 1994), neuroscience (Smith and Brown 2003), and atmospheric science (Hughes et al. 1999), beyond ecology. Our regularization strategy is most useful for applications with gradually changing states relative to the frequency of data collection, although inference can be made on the latent states and the associated probabilities regardless of transition rate.

Declarations
Conflict of interest The authors have no relevant financial or non-financial interests to disclose.
Data Availability The datasets generated and analysed during the current study will be available on ScienceBase: https://www.sciencebase.gov/catalog/item/5f62407d82ce38aaa236148b.

[Received July 2023. Revised December 2023. Accepted February 2024. Published Online April 2024.]

APPENDIX A: SIMULATION STUDY

We generated count data from $n = 20$ sites for $T = 10$ years. For $i = 1, \ldots, 20$ and $t = 1, \ldots, 10$, we simulated covariates $\boldsymbol{x}_i = \left(1, x_{i,1}, x_{i,2}\right)'$ and $\boldsymbol{h}_{i,t} = \left(h_{i,t,1}, h_{i,t,2}\right)'$ from independent standard normal distributions. To specify the latent trajectory, we let $\boldsymbol{m}_i = \boldsymbol{x}_i$ for the initial conditions. We simulated a continuous driver covariate, $w_{i,1}(\tau)$, by sampling from independent standard normal distributions, and an indicator driver covariate, $w_{i,2}(\tau)$, by sampling from independent Bernoulli distributions with probability 0.1. Further, we generated spatially correlated random effects, $\boldsymbol{\epsilon}_{t,q} = \left(\epsilon_{1,t,q}, \ldots, \epsilon_{10,t,q}\right)'$, $q = 1, 2$, using Equation 6. We calculated state probabilities, $\rho_{i,t,q}$, using Equation 4, and generated $z_{i,t,q} \sim \text{Bern}\left(\rho_{i,t,q}\right)$. We calculated population densities, $\lambda_{i,t}$, using Equation 3, and generated true abundance, $N_{i,t}$, using Equation 2, where we let $A_i = 1$ for all sites. Finally, we generated observed counts, $y_{i,t,j}$, $j = 1, 2, 3$, using Equation 1.

In terms of model fitting, we first selected the optimal tuning parameter from $\boldsymbol{c} = (0, 0.5, 1, 1.5, 2)'$. The array was concluded from the iterative selection process described in Section 2.2. We conducted a three-fold cross-validation, where at each non-overlapping fold, we randomly designated two-thirds of the simulated counts as the training set and the remaining one-third as the test set. We fit the models under different penalties to the training sets and evaluated their predictive performance on the test sets using the procedure described in Section 3.2. We then fit the best predictive model to all simulated data and summarized marginal posterior distributions. We repeated the above data simulation and model fitting processes twenty times to derive the empirical coverage rate of the inferred 95% credible intervals (Table 2).

REFERENCES

Ashcroft MB (2010) Identifying refugia from climate change. J Biogeogr 37:1407–1413

Berliner LM (1996) Hierarchical Bayesian time series models. In: Maximum entropy and Bayesian methods: Santa Fe, New Mexico, USA, 1995 Proceedings of the fifteenth international workshop on maximum entropy and bayesian methods, pp 15–22. Springer

Bradshaw WE, Holzapfel CM (2006) Evolutionary response to rapid climate change. Science 312:1477–1478

Burden F, Winkler D (2009) Bayesian regularization of neural networks. Methods Appl Artif Neural Netw 23–42

Carline RF, McCullough BJ (2003) Effects of floods on brook trout populations in the Monongahela National Forest, West Virginia. Trans Am Fish Soc 132:1014–1020

Chakraborty A, Gelfand AE, Wilson AM, Latimer AM, Silander JA (2011) Point pattern modelling for degraded presence-only data over large regions. J R Stat Soc Ser C Appl Stat 60:757–776

Dakos V, Matthews B, Hendry AP, Levine J, Loeuille N, Norberg J, Nosil P, Scheffer M, De Meester L (2019) Ecosystem tipping points in an evolving world. Nat Ecol Evol 3:355–362

Dunham JB, Young MK, Gresswell RE, Rieman BE (2003) Effects of fire on fish populations: landscape perspectives on persistence of native fishes and nonnative fish invasions. For Ecol Manag 178:183–196

Elwood JW, Waters TF (1969) Effects of floods on food consumption and production rates of a stream brook trout population. Trans Am Fish Soc 98:253–262

Farr MT, Green DS, Holekamp KE, Zipkin EF (2021) Integrating distance sampling and presence-only data to estimate species abundance. Ecology 102:e03204

Felus YA, Saalfeld A, Schaffrin B (2005) Delaunay triangulation structured kriging for surface interpolation. Surv Land Inf Sci 65:27

Fletcher RJ Jr, Hefley TJ, Robertson EP, Zuckerberg B, McCleery RA, Dorazio RM (2019) A practical guide for combining data to model species distributions. Ecology 100:e02710

Girosi F, Jones M, Poggio T (1995) Regularization theory and neural networks architectures. Neural Comput 7:219–269

Glauber RJ (1963) Time-dependent statistics of the Ising model. J Math Phys 4:294–307

Griffith DA (2020) Some guidelines for specifying the geographic weights matrix contained in spatial statistical models 1. In: Practical handbook of spatial statistics, pp 65–82. CRC press

Gunderson LH (2000) Ecological resilience: in theory and application. Annu Rev Ecol Syst 31:425–439

Habera JW, Kulp MA, Moore SE, Henry TB (2010) Three-pass depletion sampling accuracy of two electric fields for estimating trout abundance in a low-conductivity stream with limited habitat complexity. N Am J Fish Manag 30:757–766

Hakala JP, Hartman KJ (2004) Drought effect on stream morphology and brook trout (*Salvelinus fontinalis*) populations in forested headwater streams. Hydrobiologia 515:203–213

Hamilton JD (1994) State-space models. Handb Econ 4:3039–3080

Hans C (2009) Bayesian lasso regression. Biometrika 96:835–845

Hare DK, Benz SA, Kurylyk BL, Johnson ZC, Terry NC, Helton AM (2023) Paired air and stream temperature analysis (PASTA) to evaluate groundwater influence on streams. Water Resources Research page e2022WR033912

Hastie T, Mallows C (1993) A statistical view of some chemometrics regression tools: discussion. Technometrics 35:140–143

Hazzard A (1932) Some phases of the life history of the eastern brook trout, *Salvelinus fontinalis* Mitchell. Trans Am Fish Soc 62:344–350

Hefley TJ, Broms KM, Brost BM, Buderman FE, Kay SL, Scharf HR, Tipton JR, Williams PJ, Hooten MB (2017) The basis function approach for modeling autocorrelation in ecological data. Ecology 98:632–646

Hooten MB, Hobbs NT (2015) A guide to Bayesian model selection for ecologists. Ecol Monogr 85:3–28

Hudy M, Thieling TM, Gillespie N, Smith EP (2008) Distribution, status, and land use characteristics of subwatersheds within the native range of brook trout in the eastern United States. N Am J Fish Manag 28:1069–1085

Hughes JP, Guttorp P, Charles SP (1999) A non-homogeneous hidden Markov model for precipitation occurrence. J R Stat Soc Ser C Appl Stat 48:15–30

Isaac JL, De Gabriel JL, Goodman BA (2008) Microclimate of daytime den sites in a tropical possum: implications for the conservation of tropical arboreal marsupials. Anim Conserv 11:281–287

Jia X, Willard J, Karpatne A, Read JS, Zwart JA, Steinbach M, Kumar V (2021) Physics-guided machine learning for scientific discovery: an application in simulating lake temperature profiles. ACM/IMS Trans Data Sci 2:1–26

Johnson DS, Laake JL, Ver Hoef JM (2010) A model-based approach for making ecological inference from distance sampling data. Biometrics 66:310–318

Johnstone JF, Allen CD, Franklin JF, Frelich LE, Harvey BJ, Higuera PE, Mack MC, Meentemeyer RK, Metz MR, Perry GL, Schoennagel T (2016) Changing disturbance regimes, ecological memory, and forest resilience. Front Ecol Environ 14:369–378

Kanno Y, Letcher BH, Hitt NP, Boughton DA, Wofford JE, Zipkin EF (2015) Seasonal weather patterns drive population vital rates and persistence in a stream fish. Glob Change Biol 21:1856–1870

Kanno Y, Kulp MA, Moore SE (2016) Recovery of native Brook Trout populations following the eradication of nonnative Rainbow Trout in southern Appalachian Mountains streams. N Am J Fish Manag 36:1325–1335

Kanno Y, Kulp MA, Moore SE, Grossman GD (2017) Native brook trout and invasive rainbow trout respond differently to seasonal weather variation: spawning timing matters. Freshw Biol 62:868–879

Keppel G, Van Niel KP, Wardell-Johnson GW, Yates CJ, Byrne M, Mucina L, Schut AG, Hopper SD, Franklin SE (2012) Refugia: identifying and understanding safe havens for biodiversity under climate change. Glob Ecol Biogeogr 21:393–404

Kleinhesselink AR, Adler PB (2018) The response of big sagebrush (*Artemisia tridentata*) to interannual climate variation changes across its range. Ecology 99:1139–1149

Loarie SR, Duffy PB, Hamilton H, Asner GP, Field CB, Ackerly DD (2009) The velocity of climate change. Nature 462:1052–1055

Lu X, Hooten MB, Raiho AM, Swanson DK, Roland CA, Stehn SE (2023) Latent trajectory models for spatio-temporal dynamics in Alaskan ecosystems. Biometrics

Merriam ER, Fernandez R, Petty JT, Zegre N (2017) Can brook trout survive climate change in large rivers? If it rains. Sci Total Environ 607:1225–1236

Mohankumar NM, Hefley TJ, Silber KM, Boyle WA (2023) Data fusion of distance sampling and capture–recapture data. Spat Stat 55:100756

Mork D, Wilson A (2022) Treed distributed lag nonlinear models. Biostatistics 23:754–771

Morris JS (2015) Functional regression. Annu Rev Stat Appl 2:321–359

Ogle K, Barber JJ, Barron-Gafford GA, Bentley LP, Young JM, Huxman TE, Loik ME, Tissue DT (2015) Quantifying ecological memory in plant and ecosystem processes. Ecol Lett 18:221–235

Park T, Casella G (2008) The Bayesian lasso. J Am Stat Assoc 103:681–686

Peltier DM, Barber JJ, Ogle K (2018) Quantifying antecedent climatic drivers of tree growth in the Southwestern US. J Ecol 106:613–624

Polson NG, Scott JG (2010) Shrink globally, act locally: sparse Bayesian regularization and prediction. Bayesian Stat 9:105

Raiho AM, Scharf HR, Roland CA, Swanson DK, Stehn SE, Hooten MB (2022) Searching for refuge: a framework for identifying site factors conferring resistance to climate-driven vegetation change. Divers Distrib 28:793–809

Ramsay JO, Dalzell CJ (1991) Some tools for functional data analysis. J R Stat Soc Ser B (Methodol) 53:539–561

Renner IW, Elith J, Baddeley A, Fithian W, Hastie T, Phillips SJ, Popovic G, Warton DI (2015) Point process models for presence-only analysis. Methods Ecol Evol 6:366–379

Roghair CN, Dolloff CA, Underwood MK (2002) Response of a brook trout population and instream habitat to a catastrophic flood and debris flow. Trans Am Fish Soc 131:718–730

Royle JA (2004) N-mixture models for estimating population size from spatially replicated counts. Biometrics 60:108–115

Scharf HR, Raiho AM, Pugh S, Roland CA, Swanson DK, Stehn SE, Hooten MB (2022) Multivariate Bayesian clustering using covariate-informed components with application to boreal vegetation sensitivity. Biometrics 78:1427–1440

Skelly DK, Joseph LN, Possingham HP, Freidenburg LK, Farrugia TJ, Kinnison MT, Hendry AP (2007) Evolutionary responses to climate change. Conserv Biol 21:1353–1355

Smith AC, Brown EN (2003) Estimating a state-space model from point process observations. Neural Comput 15:965–991

Thornton M, Shrestha R, Wei Y, Thornton P, Kao S, Wilson B (2022) Daymet: daily surface weather data on a 1-km grid for North America, Version 4 R1. ORNL DAAC, Oak Ridge

Tibshirani R (1996) Regression shrinkage and selection via the lasso. J R Stat Soc Ser B (Methodol) 58:267–288

U.S. Geological Survey (2016). NHDPlus Version 2

Wadsworth C, Vera F, Piech C (2018) Achieving fairness through adversarial learning: an application to recidivism prediction. arXiv:1807.00199

Warren DR, Robinson JM, Josephson DC, Sheldon DR, Kraft CE (2012a) Elevated summer temperatures delay spawning and reduce redd construction for resident brook trout (*Salvelinus fontinalis*). Glob Change Biol 18:1804–1811

Warren J, Fuentes M, Herring A, Langlois P (2012b) Spatial–temporal modeling of the association between air pollution exposure and preterm birth: identifying critical windows of exposure. Biometrics 68:1157–1167

Wikle CK, Berliner LM, Cressie N (1998) Hierarchical Bayesian space–time models. Environ Ecol Stat 5:117–154

Williams PM (1995) Bayesian regularization and pruning using a Laplace prior. Neural Comput 7:117–143

Williams SE, Shoo LP, Isaac JL, Hoffmann AA, Langham G (2008) Towards an integrated framework for assessing the vulnerability of species to climate change. PLoS Biol 6:e325

Wood DM, Welsh AB, Todd Petty J (2018) Genetic assignment of brook trout reveals rapid success of culvert restoration in headwater streams. N Am J Fish Manag 38:991–1003

Wu F-Y (1982) The Potts model. Rev Mod Phys 54:235

Xu C, Letcher B, Nislow K (2010a) Size-dependent survival of brook trout *Salvelinus fontinalis* in summer: effects of water temperature and stream flow. J Fish Biol 76:2342–2369

Xu C, Letcher BH, Nislow KH (2010b) Context-specific influence of water temperature on brook trout growth rates in the field. Freshw Biol 55:2253–2264

Zucchini W, MacDonald IL, Langrock R (2017) Hidden Markov models for time series: an introduction using R. CRC Press, Cambridge